Characterization of *a*-Si:H/*a*-Ge:H superlattices by Raman scattering

P. V. Santos and L. Ley
Max-Planck-Institut für Festkörperforschung, Heisenbergstrasse 1, D-7000 Stuttgart 80, Federal Republic of Germany
(Received 17 February 1987)

We have investigated the vibrational spectra of *a*-Si:H/*a*-Ge:H superlattices by Raman scattering. For high frequencies (>100 cm^{-1}) the intensity of the Raman spectrum is proportional to the density of vibrational states and shows contributions from the Si—Si and Ge—Ge bonds within the superlattice layers and from the Si—Ge bonds in the interface region. From the relative intensities of these modes we determine the individual layer thicknesses and the width of the interface. These results are discussed in terms of the growth conditions. For low frequencies (<80 cm^{-1}) the Raman spectra show peaks corresponding to the excitation of folded-zone longitudinal acoustic phonons. The dispersion relation for these phonons is determined by measuring the peak positions as a function of laser energy and of the superlattice period. The result is well described by a continuum elastic model. The linewidth of these peaks increases with phonon frequency, indicating that the dispersion relation acquires a non-negligible imaginary component due to the loss of phase coherence of the acoustic vibrations.

I. INTRODUCTION

Periodic structures consisting of alternating layers of amorphous semiconductors have been fabricated recently.[1–4] These structures combine the isotropy and homogeneity of the amorphous material within each layer with an artificial periodicity in the direction perpendicular to the layers as imposed by the growth process. These two aspects of the so-called amorphous superlattices are reflected in their Raman spectrum, as shown in Fig. 1. For high-frequency vibrations (>60 cm^{-1}), the characteristic distance over which the phase coherence of the vibration is maintained is very small compared to the exciting-light wavelength used in Raman scattering. This is a result of the lack of long-range order in the amorphous material. The vibrational modes, which we will also denote by phonons in analogy to the crystalline vibrations, can therefore not be characterized by a well-defined wave vector **Q** in this frequency range. Consequently, in a Raman experiment the momentum conservation rule is relaxed and all photon modes contribute to the first-order Raman scattering. Except for a Bose-Einstein population factor and for a slowly varying, frequency-dependent light scattering probability for phonons, the Raman spectrum is thus proportional to the density of vibrational states and therefore to the total number of scatterers present in the sample.[5] In a multilayer structure, the Raman spectrum will be a superposition of the Raman spectra of the individual layers weighted by the scattering probability for phonons of each material. As the repetition period of the multilayer decreases, the number of interface bonds becomes a significant fraction of the total number of bonds. In *a*-Si/*a*-Ge superlattices, the characteristic Si-Si, Ge-Ge, and Si-Ge modes are sufficiently separated in energy to allow an investigation of the chemical compositions of the interfaces by Raman scattering.[6,7] This was first demonstrated by Persans *et al.*[6] and we perform a similar analysis of our samples in Sec. III.

The influence of the artificial periodicity on the vibrational spectrum of an amorphous superlattice becomes apparent for low-frequency acoustic vibrations (<80 cm^{-1}), where the phase coherence length of the phonons exceeds the superlattice period. These vibrations involve the nearly in-phase movement of neighboring atoms and their coherence length is less sensitive to the lack of long-range order as compared with optical vibrations. In fact, for very low frequencies, the phonons are well described by elastic sound waves propagating in a continuous medium with a constant velocity. Under these conditions the momentum conservation rule for light scattering restricts the scattering to discrete frequencies that are observed in

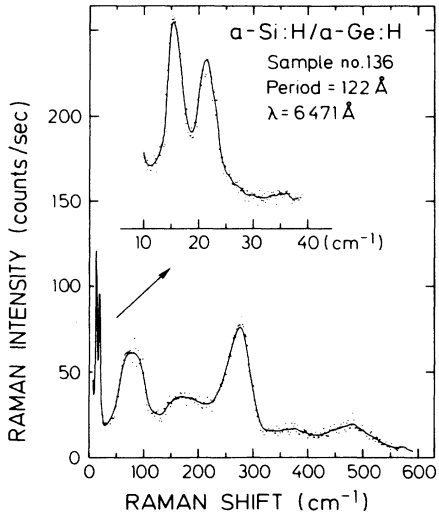

FIG. 1. Raman spectrum of an *a*-Si:H/*a*-Ge:H superlattice with a period of 122 Å. An expansion of the low-frequency region of the spectrum shows the excitations of the first zone-folded LA phonons.

Brillouin spectroscopy.[8] In a superlattice, the periodic modulation of the acoustic properties allows for the possibility of umklapp scattering for phonons propagating perpendicular to the layers. The umklapp vectors are integer multiples of $2\pi/d$, where d is the repetition period. This restricts the magnitude of the irreducible phonon wave vector q to a mini-Brillouin-zone of dimension $2\pi/d$. The phonon dispersion is, to a first approximation, obtained by folding into this mini-Brillouin-zone the acoustic phonon branch of an unstructured material with an effective sound velocity that depends on the superlattice composition.[9] Higher-folded phonon branches are accessible in light scattering experiments in addition to the lowest branch that is observed in Brillouin scattering from unstructured materials.[10,11] The excitation of longitudinal acoustic (LA) folded phonons is evidenced by the two sharp peaks in the low-frequency range of the Raman spectrum of Fig. 1(a). We shall present in Sec. IV a comprehensive study of the frequency of the folded-zone LA phonons in a-Si/a-Ge superlattices as a function of the phonon wave vector and the superlattice period.

As the phonon frequency increases the phase coherence length is reduced. This is reflected in the broadening of the Raman peaks associated with folded phonons. We investigate the frequency and the temperature dependence of the linewidth broadening in Sec. V. Possible mechanisms for the broadening are discussed.

II. SAMPLE PREPARATION

The a-Si:H/a-Ge:H superlattices were prepared in a computer-controlled capacitive glow-discharge reactor described elsewhere.[12] The samples have periods ranging from 27 to 232 Å and a total thickness between 0.5 and 1.0 μm. Pure silane was used to deposit the a-Si:H layers, and the a-Ge:H layers were grown from GeH_4 (one part per volume) diluted in Ar (10 parts per volume). The other deposition conditions were a pressure of 0.25 mbar in the discharge chamber, a substrate temperature of 200 °C, a total gas flow of 4 sccm (cm^3/min at room temperature and 760 torr) and a rf power density of 40 mW/cm^2. A rectangular composition profile was achieved by alternating the gas composition in the discharge chamber periodically without extinguishing the plasma. In order to minimize cross contamination due to the 3 s residence time of the gases in the discharge chamber, an argon plasma was maintained for 15 s after the deposition of each layer.

The thickness of an individual layer was determined by the deposition time of thick ($\sim$0.4 μm) homogeneous films; their thickness was subsequently measured by a profilometer. We measured growth rates of $g_{Si}=1.0$ Å/s and $g_{Ge}=1.2$ Å/s under the conditions mentioned above.

The samples used in this study are listed in Table I. The first three specimens (nos. 132, 133, and 140) are unstructured films used as references. The composition $x=0.57$ of the a-Si_xGe_{1-x}:H sample was determined by comparing its optical gap with that of alloy samples of known composition.[13] An a-Si:H sample, where the SiH_4 flow was interrupted every 15 s to be replaced by argon for 15 s (sample no. 144), was prepared to study the effect of the Ar plasma on a nominally unstructured film. The remainder of the samples (nos. 134–139 and no. 141) are superlattices. Their periods, d (third column of Table I), were determined by dividing the total thickness of each sample by the number of deposition cycles.

The deposition times of each layer t_{Ge} and t_{Si} were adjusted so as to maintain nominally a constant thickness ratio $d_{Ge}/d_{Si}=r=0.80$ independent of the superlattice period. However, the actual thickness ratio is not constant because it turns out that the layers continue to grow during the Ar plasma period. This becomes evident if we consider the average growth rate defined as

$$g \equiv \frac{d}{t_{Si}+t_{Ge}} . \quad (1)$$

Values for g are listed in the fourth column of Table I for each sample. For unstructured samples g is simply the ratio between the thickness and the deposition time. In the ideal case where the gases are changed instantaneously, g should be independent of the period for fixed deposition time ratios t_{Ge}/t_{Si}. This remains valid for finite gas-changing times if the growth rate of silicon (germanium) is proportional to the partial pressure of silane (germane)

TABLE I. The samples used in this study.

Sample number	Thickness (μm)	Period d (Å)	Average growth rate g (Å/s)	d_{Si} (Å)	d_{Ge} (Å)	$2d_{Si\text{-}Ge}$ (Å)	Sample type
132	0.43		1.2				a-Si:H
133	0.37		1.0				a-Ge:H
140	1.40		1.6				a-$Si_{0.57}Ge_{0.43}$:H
144	0.77	32	2.14				a-Si:H/Ar
134	0.72	232	1.14	122	95	15	a-Si:H/a-Ge:H
135	0.56	187	1.22	102	70	15	
136	0.76	122	1.20	62	45	15	
137	0.84	94	1.32	49	30	15	
138	0.82	63	1.53	33	15	15	
141	0.75	37	1.83	17	5	15	
139	0.72	27	2.61	11	1	15	

in the deposition chamber. In this case the variations in the growth rates due to transient conditions at the beginning and the end of a layer compensate each other exactly, leaving no net effect on the layer thickness. Contrary to this expectation, the average growth rate g in Table I increases with decreasing superlattice period. In fact, the growth rate of the a-Si:H sample No. 144, where the SiH_4 flow was interrupted and replaced by Ar, is much higher than that of sample no. 133, which was grown without interruption of the silane flow.

The high growth rates of the superlattices cannot be explained by transient variations of the pressure or rf power during the gas changes. These variations are kept between -8% and $+15\%$ for the pressure, and within $\pm 2\%$ for the rf power. We attribute the high average growth rate of the a-Si:H sample no. 144 (Table I) to the continuation of the film growth when silane is diluted in argon during the switchover from SiH_4 to Ar and from Ar to SiH_4. From the thickness of sample no. 144 and the fact that $g_{Si}=1.0$ Å/s for unstructured a-Si:H we deduce that an additional 17 Å of a-Si:H grow per period during the argon-purging intervals.

The connection between growth rate and superlattice period can now be understood in terms of a simple model, where the thickness of each period is assumed to exceed the value determined from the deposition rates of a-Si:H and a-Ge:H by a constant thickness d_a. In this case we have for the average growth rates

$$g=\frac{t_{Si}g_{Si}+t_{Ge}g_{Ge}+d_a}{t_{Si}+t_{Ge}} =\frac{g_{Si}+rg_{Ge}}{1+r}+\frac{d_a}{t_{Si}+t_{Ge}}\ , \tag{2}$$

where $(g_{Si}+rg_{Ge})/(1+r)=1.1$ Å/s for all our superlattices with $r=0.80$.

Figure 2 shows a plot of g versus $1/(t_{Si}+t_{Ge})$ for the superlattices considered in this work. The points are well fitted by a straight line which crosses the vertical axes at $g=1.1\pm0.1$ Å/s in agreement with Eq. (2). From the slope of this line we determine $d_a=15.5\pm1$ Å.

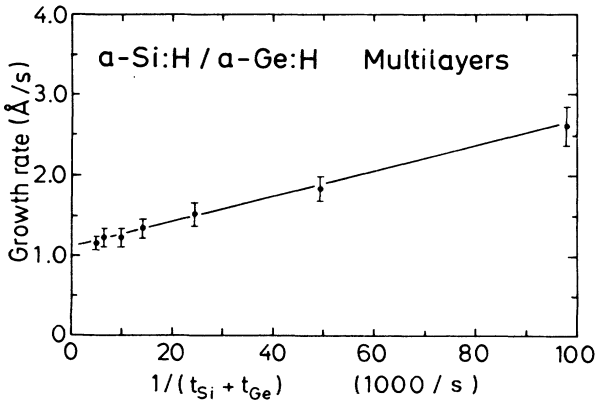

FIG. 2. The growth rate of the superlattices vs the inverse of the sum of the deposition time for the silicon (t_{Si}) and for the germanium (t_{Ge}) layers.

This value is so close to the additional thickness of 17 Å per period determined in the a-Si:H/Ar sample (no. 144) that it is safe to assume that the additional thickness is solely due to silicon. This indicates also that the growth rate of a-Ge:H is proportional to the GeH_4 concentration in argon for concentrations below 10%.

The nonreciprocity between deposition rates and SiH_4 concentration in inert gases has been previously recognized.[14–16] For low power discharges Street *et al.*[15] reported deposition rates for a-Si:H that are independent of the silane concentration $[SiH_4]$ in argon down to a volume fraction $[SiH_4]/[Ar]=0.1\%$. Kampas[16] has studied the kinetics of a-Si:H deposition from argon-silane mixture by means of optical emission spectroscopy. He developed a model in which the growth rate of a-Si:H is proportional to the product $k_d n_e[SiH_4]$, where k_d depends on the electron energy distribution in the plasma and n_e is the electron density. At low SiH_4 partial pressures n_e increases faster than $[SiH_4]^{-1}$, as the silane concentration decreases. The average electron energy and consequently k_d also increase with $[SiH_4]$. The net effect is a deposition rate that is highest for a silane dilution of $\sim 2\%$.

III. RAMAN SCATTERING: HIGHER-FREQUENCY REGION

The Raman measurements reported here were performed in the backscattering configuration with p-polarized light impinging on the sample at an angle of 45°. A constant power level of 150 mW was used for all samples. The scattered light emerging perpendicular to the sample surface was collected and analyzed in a Jarrel-Ash triple monochromator. The samples were kept in vacuum (below 10^{-5} torr) and at room temperature, except for the heating due to the incident light.

Figure 3 shows the Raman spectra of a series of samples. Figure 3(a) is the Raman spectrum of pure a-Ge:H (sample no 132 of Table I). The two main peaks at 80 and 275 cm^{-1} are due to maxima in the density of vibrational states (DOS) corresponding to the TA and TO phonons in the crystal, respectively.[17] For a-Si:H sample no. 144 [Fig. 3(b)], the corresponding peaks lie at 160 and 480 cm^{-1}, respectively.[18] The broad maxima between the two main peaks correspond to the excitations of LA-like and LO-like phonons in both spectra. The Raman spectra of large-period superlattices in Fig. 3 are basically the superposition of the a-Si:H and a-Ge:H spectra as shown for sample no 138 ($d=63$ Å) in Fig. 3(c). As the superlattice period decreases the relative contribution due to the heteropolar Si—Ge bonds at the interfaces increases with respect to the spectral features of pure silicon and pure germanium as judged by the growing influence of Si-Ge Raman modes at 380 cm^{-1} in Figs. 3(d) and 3(e). The other main Si-Ge vibrational modes are identified in the Raman spectrum of the a-$Si_{0.57}Ge_{0.43}$:H sample [Fig. 3(f)]. There are two maxima at 100 and 250 cm^{-1} which bear a certain relationship to the corresponding modes at 80 and 270 cm^{-1} in the spectra of pure a-Ge:H. The TO maximum of the Si network finds its corresponding feature in the shoulder at about 460 cm^{-1} in the alloy. The details of the origin of these modes are discussed elsewhere.[19]

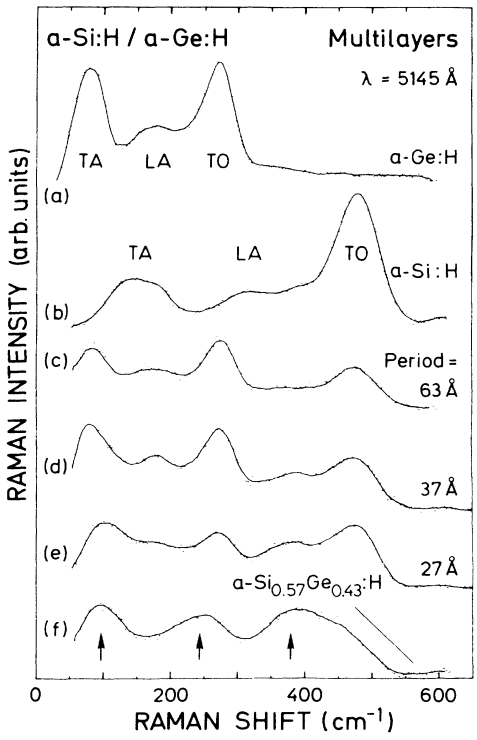

FIG. 3. Raman spectra of (a) a-Ge:H, (b) a-Si:H, (c)–(e) a-Si:H/a-Ge:H superlattices, and (f) a-$Si_{0.57}Ge_{0.43}$:H alloy. The arrows on the latter curve indicate the characteristic Si-Ge vibrations modes that are not present in the spectrum of pure a-Si:H or a-Ge:H.

In order to relate the Raman spectrum of the superlattice to the Raman spectra of the unstructure layers we follow the procedure of Persans *et al.*[6] A four-layer model is assumed for the superlattice a-Si:H/a-Si_xGe_{1-x}:H/a-Ge:H/a-Si_xGe_{1-x}:H with $x\sim 0.5$. The intensity of the features in the Raman spectrum associated with Si-Si, Ge-Ge, and Si-Ge optical modes is related to the total number of bonds of each type and therefore to the thickness of the layers. The Raman spectrum is a linear combination of the Raman spectra of the individual layers which are measured separately in unstructured samples. The decomposition is expressed by

$$I_{SL}(\omega)\sim(2\alpha_{Si}L_{Si})I_{Si}(\omega)+(2\alpha_{Ge}L_{Ge})I_{Ge}(\omega) +(4\alpha_{Si\text{-}Ge}L_{Si\text{-}Ge})I_{Si\text{-}Ge}(\omega)\ , \quad (3)$$

where $I(\omega)$ is the measured Raman intensity, L is proportional to the layer thickness, and α is the light absorption coefficient of the layers. The subscripts Si, Ge, Si-Ge, and SL refer, respectively, to the silicon, germanium, the silicon-germanium interface layer, and to the superlattice. This expression is valid if the penetration depth of the laser light in the sample is much larger than the superlattice period. By decomposing the Raman spectra of the superlattice into these three contributions we derive values for the parameters L. These values are then normalized to the known superlattice period to obtain the "spectroscopic" thickness of the individual layers

$$d^R_{Si}=dL_{Si}/(L_{Si}+L_{Ge}+L_{Si\text{-}Ge})\ . \quad (4)$$

Similar expressions apply for the a-Ge and a-Si_xGe_{1-x} layers. The "spectroscopic thicknesses" determined in this way are to be understood as the thickness of the corresponding unstructured material containing, per unit area, the same number of scattering centers as the superlattice period.

Samples 132 (a-Ge:H), 144 (a-Si:H), and 140 (a-$Si_{0.57}Ge_{0.43}$:H) of Table I were used as a reference for the decomposition of the Raman spectra of the superlattices. The Raman measurements were made with an excitation wavelength of 5145 Å (2.41 eV) and 6471 Å (1.92 eV). Light with these energies is mainly absorbed in the a-Ge:H layers with its smaller band gap and an absorption coefficient of 10^4 cm^{-1} for the energy $E_{04}=1.1$ eV. From the absorption coefficient of a-Ge:H we estimate a mean penetration depth of ~ 100 Å and ~ 300 Å for these two wavelengths, respectively. The information obtained from the measurements with $\lambda=5145$ Å for small-period superlattices (period <100 Å) can then be extended to the large-period structures using the measurements with $\lambda=6471$ Å.

The decomposition of the Raman spectrum of the superlattice according to Eq. (3) was made by a least-squares fitting procedure for frequencies in the range from 200 to 600 cm^{-1} as is shown in Fig. 4. The same figure also presents the relative contributions of the individual layers to the Raman spectrum. The results of the calculation of the "spectroscopic" layer thicknesses are summarized in Fig. 5. In Fig. 5(a) we plot the "spectroscopic" width of the germanium layers (d^R_{Ge}) and twice the "spectroscopic" width of the alloy interface ($2d^R_{Si\text{-}Ge}$) versus the nominal thickness of the germanium layer, as calculated from the growth rate (g_{Ge}) and the deposition

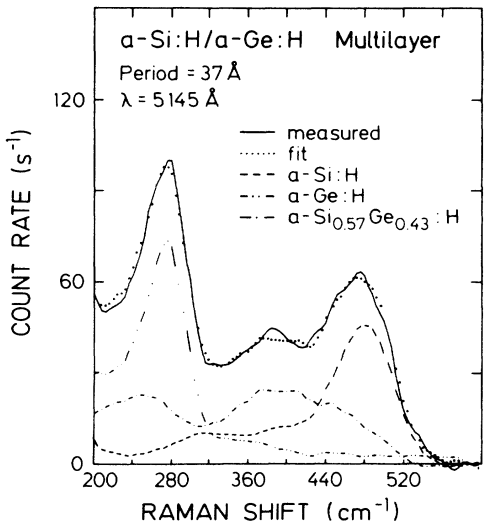

FIG. 4. Raman spectrum of an amorphous superlattice with a 37 Å period (solid line). The dotted curve is the result of the fitting procedure described in the text. The other curves show the relative contributions from the a-Si:H (— — —), the a-Ge:H (–··–··), and the a-Si_xGe_{1-x}:H (—·—·—·) interface layers.

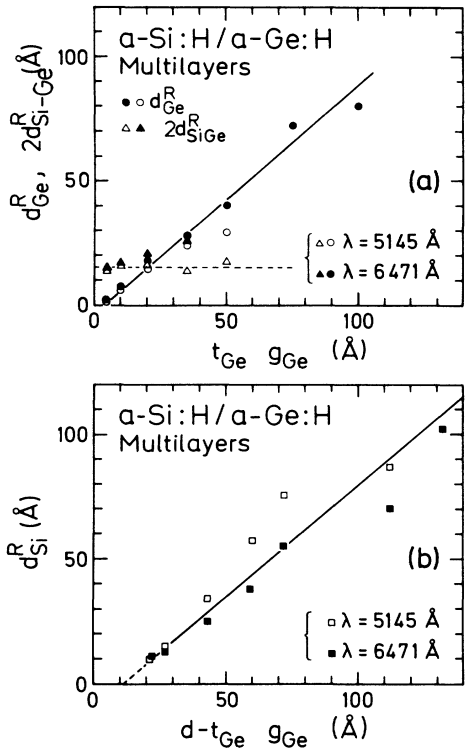

FIG. 5. (a) Dependence of the "spectroscopic" thickness of the a-Ge:H (d^R_{Ge}) and a-Si_xGe_{1-x}:H ($d^R_{Si\text{-}Ge}$) layers on the nominal thickness of the a-Ge:H layers ($t_{Ge}g_{Ge}$). (b) "Spectroscopic" thickness of the a-Si:H layers (d^R_{Si}) vs the thickness of the silicon layers as determined from the growth rates of the superlattices.

time (t_{Ge}) (see Sec. II). In Fig. 5(b) the "spectroscopic" width of the silicon layer d^R_{Si} as derived from the fit to the Raman spectra is plotted versus the silicon-layer thickness as derived from the known superlattice period and the nominal germanium width $d - t_{Ge}g_{Ge}$. The thickness of interface material in Fig. 5(a) is independent of the superlattice period and equal to 7.5±2 Å per interface ($2d_{Si\text{-}Ge} \approx 15$ Å). Both the germanium and silicon thicknesses increase linearly with $t_{Ge}g_{Ge}$ and $d - t_{Ge}g_{Ge}$, and intersect the abscissa for thickness values of 5±2 Å and 10±2 Å, respectively. We attribute these nonzero values to the consumption of silicon and germanium needed to grow the Si-Ge interface layer of 15 Å per period. In fact, if we assume the density ratio between the amorphous and crystalline phase to be the same for germanium, for silicon, and for silicon-germanium alloys then germanium and silicon layers 9 and 6 Å wide, respectively, are necessary to grow an a-$Si_{0.57}Ge_{0.43}$:H layer 15 Å wide.

The interface thickness of 7.5 Å essentially agrees with the 5.5 Å determined by Persans *et al.*[6] This corresponds to 3.5×10^{15} and 2.6×10^{15} Si—Ge bonds per cm^2 and per interface, respectively. Taking the complexity of the analysis and the uncertainty of about 20% into consideration we do not regard this difference in the interface width as significant. The authors of Ref. 6 interpreted their results in terms of a disordered monolayer of 50% Si and 50% Ge atoms created at each interface. A second disordered monolayer of the same composition would explain our data. Prokes and Spaepen[20] have recently measured the interdiffusion coefficient in a-Si/a-Ge multilayers in the low-temperature region (550–630 K). Extrapolating their results to the deposition temperature of our multilayers (200 °C = 473 K) we obtain negligible values (< 1 Å) for the interface thickness due to interdiffusion. The purging of the reactor with argon after each layer should strongly reduce the interface mixing due to simultaneous deposition from the gas phase. A possible explanation for the interface mixing lies in the surface reactions during film growth. It has recently been suggested that hydrogen elimination and crosslinking of the silicon network during a-Si:H growth occurs not only at the surface but also within a thin transition layer below the surface.[21] The material in this layer is not in its final configuration and can therefore interact with freshly deposited a-Ge:H to form an alloy interface layer. The same can also occur when silicon is deposited on germanium.

A linear regression of the data points in Figs. 5(a) and 5(b) yields slopes of 0.9±0.1 for both germanium and silicon thickness. These values are close to unity and thus support our conclusion that the Ge growth does not continue during the Ar plasma.

The results of this section allow us to define a model for the superlattice consisting of four layers: a silicon, a germanium, and two a-$Si_{0.57}Ge_{0.43}$:H layers. Each alloy layer is 7.5 Å wide. The thickness of the silicon and germanium layers will be considered to be, respectively, 10 and 5 Å thinner than their nominal values as determined in Sec. I with the understanding that the missing material is used to form the interface layers. The actual layer thicknesses of the samples used in this work are listed in columns 5 and 6 of Table I because they will be important in analyzing the results of the next sections.

IV. FOLDED ACOUSTIC PHONONS

Figure 6 shows Raman spectra obtained in the backscattering geometry for a series of a-Si:H/a-Ge:H superlattices with periods between 37 and 232 Å. Each spectrum exhibits two peaks with frequencies that increase as the superlattice period decreases. We assign these peaks to the excitation of the first (ω_{-1}) and second (ω_{+1}) folded branches of the dispersion relation for longitudinal acoustic phonons[10] propagating perpendicular to the sample surface (z direction) in analogy to similar observations made earlier in a-Si:H/a-SiN_x:H superlattices.[4] In an extended zone scheme the peaks ω_{-1} and and ω_{+1} are associated with umklapp processes involving umklapp vectors of magnitude $m(2\pi/d)$, with $m=-1$ and $m=+1$, respectively. The momentum conservation rule for the z component Q of the extended-phonon wave vector is then

$$Q = q \pm m\frac{2\pi}{d}, \quad m = \pm 1 , \tag{5}$$

where $q = 4\pi n_1/\lambda$ is the magnitude of the momentum transfer along z due to the backscattered light and n_1 is the real part of the refractive index. We verified experimentally that these peaks can only be observed for incident and scattered light polarization in the same direc-

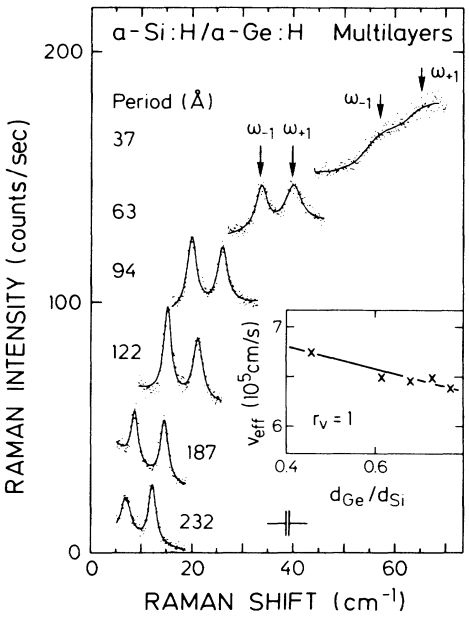

FIG. 6. Low-frequency Raman spectra of *a*-Si:H/*a*-Ge:H superlattices showing the excitation of folded LA phonons. The spectra are offset vertically for clarity. In the inset the average sound velocity of the superlattice is plotted vs the thickness ratio of the germanium and silicon layers. The solid line is a fit to the data points and yields a ratio $r_v = 1$ for the sound velocity in the amorphous phase to that of the corresponding crystalline phase along ⟨100⟩.

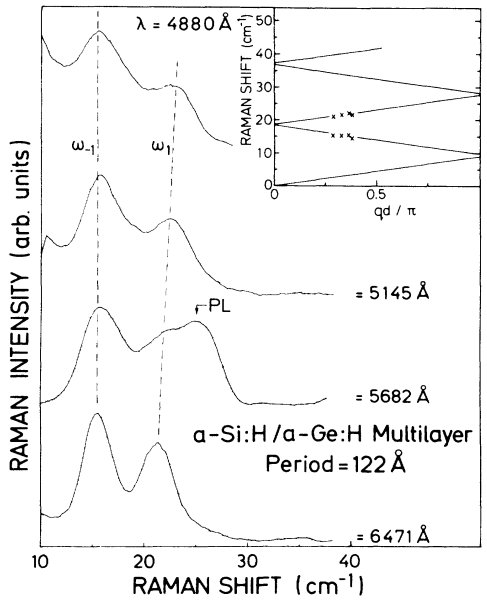

FIG. 7. Raman spectra of a superlattice recorded with different laser lines. The structure denoted by PL is a plasma line of the laser. The position of the peaks as a function of the phonon wave vector is plotted in the inset. The solid line is the calculated phonon dispersion relation using the elastic continuum model described in the text.

tion. This is in agreement with the selection rules for Raman scattering from acoustic phonons in the backscattering configuration as also observed in crystalline superlattices.[22]

The average frequency $\bar{\omega}=(\omega_1+\omega_{-1})/2$ corresponds to an extended phonon wave vector Q of magnitude $2\pi/d$ [see Eq. (4) with $q=0$]. The effective sound velocity v_{eff} for LA phonons propagating perpendicular to the layers is then given by $v_{\text{eff}}=cd\bar{\omega}$ (for $\bar{\omega}$ expressed in cm^{-1}), where c is the speed of light. This approximation for v_{eff} is valid even in the presence of frequency gaps in the dispersion relation because in this case ω_{+1} and ω_{-1} are displaced symmetrically with respect to their undisturbed values. The magnitude of v_{eff} depends on the average composition of the superlattice. In our case it is expected to vary from sample to sample because the ratio of the layer thicknesses does not remain constant as discussed in the previous sections (see Table I). In the insert of Fig. 6 we plot v_{eff} versus the thickness ratio $d_{\text{Ge}}/d_{\text{Si}}$. The slight decrease in v_{eff} with $d_{\text{Ge}}/d_{\text{Si}}$ is consistent with the fact that the sound velocity in germanium is smaller than in silicon.

We followed the folded-phonon dispersion relation ω versus q in a particular sample as a function of the wave vector q by varying the laser wavelength λ_L and thereby $q=4\pi n_1/\lambda_L$. Figure 7 shows Raman spectra recorded with different wavelengths for a 122-Å-period sample. The position of the peaks are plotted as a function of the magnitude of the phonon wave vector q in the insert of the figure. The average frequency $\bar{\omega}=(\omega_{-1}+\omega_{+1})/2$ remains constant while the frequency splitting $\omega_{+1}-\omega_{-1}$ increases with decreasing laser wavelength as one moves towards the boundary of the mini-Brillouin-zone.

In order to associate the previous results with the acoustic properties of the superlattice layers we first note that according to Eq. (5), the phonon wavelength involved in the scattering process is of the order of the superlattice period. In our sample, these periods are considerably larger than the interatomic distances and these modes involve the in-phase movement of several neighboring atoms. In this case the dynamical properties of each amorphous layer are well represented by an elastic isotropic medium characterized by a density ρ and an elastic constant c_e (Ref. 23). The long-wavelength longitudinal acoustic phonons can thus be treated as elastic waves propagating along the z direction in a layered continuum according to the one-dimensional wave equation:[24]

$$\rho(z)\omega^2=\frac{d}{dz}\left[c_e(z)\frac{du(z)}{dz}\right], \tag{6}$$

where $u(z)$ is the acoustic displacement field.

The effective sound velocity v_{eff} for a periodic layered structure is obtained from an approximate solution of Eq. (6) as[22]

$$v_{\text{eff}}^2=\frac{\sum_{i=1}^{n} d_i\rho_i v_i^2}{\sum_{i=1}^{n} d_i\rho_i}, \tag{7}$$

where d_i, v_i, and ρ_i are, respectively, the thickness, the

longitudinal sound velocity, and the density of the ith layer of the period consisting of n layers. Note that the elastic constant of layer i is equal to $\rho_i v_i^2$. In order to calculate v_{eff} for the four-layer model of our a-Si:H/a-Ge:H superlattices described in the last section we need the sound velocities and the densities of the individual layer. For the silicon and germanium layer we have assumed the longitudinal sound velocity to be proportional to the corresponding velocity in the $\langle 100 \rangle$ direction of the crystals, with a common proportionality factor r_v. In Eq. (7) the densities appear both in the numerator and denominator so that only their ratios are needed. Assuming that the ratios are the same for the amorphous and crystalline phases of germanium, silicon, and the silicon-germanium alloy, we use the crystalline densities. For the a-$Si_{1-x}Ge_x$:H interface layer we take values for the density ρ and the elastic constant ρv^2 interpolated linearly in x between the values for silicon and germanium. In this way the only adjustable parameter is the ratio of the amorphous to crystalline sound velocity r_v. A linear regression of the data points in the inset of Fig. 6 yields $r_v = 1.00 \pm 0.05$. The corresponding sound velocities for a-Si:H, a-Ge:H, and a-$Si_{0.57}Ge_{0.43}$ so obtained are, respectively, $(8.4 \pm 0.4) \times 10^5$ cm/s, $(4.9 \pm 0.3) \times 10^5$ cm/s, and $(6.4 \pm 0.3) \times 10^5$ cm/s. The longitudinal sound velocity of a-Si:H falls in the range of values determined from Brillouin scattering ($v_{\text{Si}} = 8.4 \times 10^5$ to 8.8×10^5 cm/s) for films with a hydrogen content of 15 at. % (Ref. 8). We emphasize that this is not a very viable method to determine sound velocities as long as too many assumptions concerning the relative densities and relative elastic constants have to be made. We consider it rather a demonstration that a continuum model with frequency-independent sound velocities is a reasonable approximation for the present case.

The dispersion relation of the superlattice in the long-wavelength limit is given by the solution of (6) for the modulation profile. For a periodically layered structure, these solutions are obtained by first solving the wave equation within each layer and then applying the boundary conditions to join these solutions at each interface.[25] In order to reduce the complexity resulting from the large number of layers (four layers per period) and still taking into account the interface alloy regions, we simplify the problem by combining the two interface regions into a single layer of thickness $2d_{\text{Si-Ge}}$ placed between the germanium and the silicon layer. Each period has the sequence a-Si:H/a-Ge:H/a-$Si_{0.57}Ge_{0.43}$:H. The solution of Eq. (6) for a three-layer structure gives the following expression for the dispersion relation:

$$\cos(qd) = \tfrac{1}{8}[G_1 G_2 G_3 \cos(\theta_1+\theta_2+\theta_3) + G_{-1} G_{-2} G_3 \cos(\theta_1+\theta_2-\theta_3) + G_1 G_{-2} G_{-3} \cos(\theta_1-\theta_2-\theta_3) + G_{-1} G_2 G_{-3} \cos(\theta_1-\theta_2+\theta_3)] , \tag{8}$$

where

$$G_{\pm i} = (1 \pm F_i), \quad F_i = \frac{\rho_j v_j}{\rho_k v_k}, \quad i,j,k = 1,2,3$$

and

$$\theta_i = \omega d_i / v_i .$$

For a two-layer structure, this expression reduces to Rytov's dispersion relation.[26]

Taking the sound-velocity values previously determined, we use Eq. (8) to calculate the dispersion relation of the 122-Å superlattice of Fig. 7 (sample no. 136 of Table I). The result is the continuous line in the inset of the same figure. We repeat this procedure for the other samples and always achieve good agreement between Eq. (8) and the experimentally determined dispersion relation. This shows that with respect to LA-phonon propagation the amorphous superlattices are well described by a layered continuum. Considering that the folded phonons were observed for superlattice periods smaller than 60 Å, these results demonstrate that the dispersion relation of the individual amorphous materials remain linear (constant sound velocity) up to phonon wave vectors with a magnitude that corresponds to 10% of the Brillouin zone of crystalline silicon.

In the Raman spectrum of the a-Si:H/a-Ge:H superlattices we have not been able to detect the peaks corresponding to the excitation of phonons from the higher-order $|m| > 1$ folded branches that were observed in crystalline superlattices.[22] We attribute this to the low intensity of the light scattered by these modes. The light scattering from acoustic phonons in amorphous materials results from the modulation of the electric susceptibility by the strain produced by the phonon.[27] The changes in the susceptibility are proportional to the strain, the proportionality factor being the photoelastic coefficient p. In a superlattice, the photoelastic coefficient is modulated along the growth direction. To a first approximation, the intensity of the light scattered by phonons from the mth folded branch is proportional to the square of the mth Fourier component of $p(z)$, $|P_m|^2$ (Ref. 22). For the four-layer model for the superlattices introduced in Sec. II the Fourier components are proportional to

$$|P_m|^2 \propto \frac{(p_{\text{Si}} - p_{\text{Ge}})^2}{m^2} \times \left[\sin\left[\frac{m\pi d_{\text{Si}}}{d} \right] + \sin\left[\frac{m\pi(d_{\text{Si}} + 2d_{\text{Si-Ge}})}{d} \right] \right] , \tag{9}$$

where p_{Si} and p_{Ge} are the photoelastic coefficients of the silicon and germanium layers, respectively. We have assumed in the derivation of Eq. (9) that the photoelastic coefficient of the interface a-Si_xGe_{1-x}:H layer is the average of the values for silicon and germanium, so that the modulation profile of $p(z)$ is symmetric around its average value. Equation (9) shows that the scattering intensity decreases quadratically with the branch index m. In fact, substituting the layer thicknesses for the largest-period sample (no 134 of Table I) in Eq. (9) we obtain $|P_2/P_1|^2=0.03$ and $|P_3/P_1|^2=0.08$. The intensity of the higher-order Raman peaks is therefore at least an order of magnitude smaller than that of branches $m=\pm 1$, i.e., below the detection limit of our experiments.

V. LINEWIDTH

The increase in the frequency of the folded-phonon peaks with decreasing superlattice period is accompanied by an increase in the linewidth. Moreover, the ω_{+1} peak in the small-period samples is always broader than the lower-frequency peak at ω_{-1}. The broadening effect is apparent in the series of spectra shown on Fig. 6. The linewidth increases initially slowly for phonon frequencies up to ~ 50 cm^{-1} [Figs. 6(b)–6(f)]. At ~ 50 cm^{-1}, the TA density of states starts to contribute significantly to the Raman spectrum. The folded LA phonons of the 37 Å superlattice [Fig. 6(a)] are so severely broadened that they are hardly observable on top of the TA density of states.

The linewidth is assumed to be the geometrical sum of the intrinsic linewidth Γ [full width at half maximum (FWHM)] and the spectrometer resolution. The intrinsic contribution to the width of both the ω_{-1} and ω_{+1} peaks are plotted versus ω in Fig. 8. A linear recursion of the data points for frequencies below 40 cm^{-1} yields a power-law dependence given by

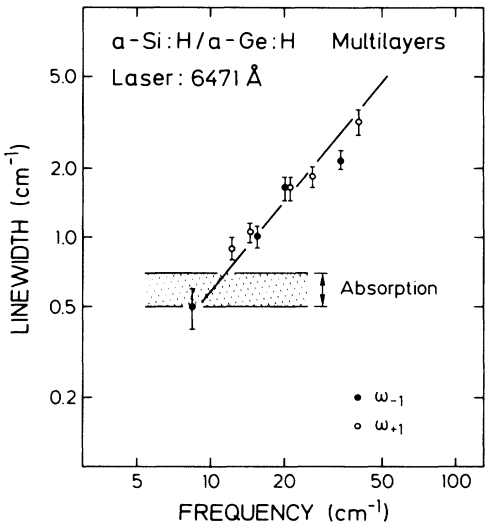

FIG. 8. Linewidth of the Raman folded-phonon peaks plotted vs the phonon frequency. The contribution of the light absorption to the linewidth lies within the hatched area for all superlattice samples.

$$\Gamma=(0.03\pm 0.005\ \text{cm}^{-1})^{-\nu}\omega^{\nu}\ , \tag{10}$$

where $\nu=1.3\pm 0.1$.

We now consider the possible mechanisms that might account for the broadening of the Raman lines. The first one is due to the laser light absorption in the opaque samples. The absorption broadens the light wave vector within the sample allowing a wider range of phonon modes to couple to the light. Away from the frequency gaps, where the dispersion relation is linear, the broadening of the Raman lines can be calculated by extending the results derived by Sandercock for the linewidth of Brillouin scattering lines.[28] The folded phonons have a Lorentzian shape with a full width at half maximum $\Delta\omega$ given by

$$\Delta\omega=2\frac{n_2}{n_1}qv_{\text{eff}}=2\alpha v_{\text{eff}}\ , \tag{11}$$

where $n=n_1+in_2$ is the complex refractive index of the sample for the laser energy, q is the magnitude of the reduced phonon wave vector, and α is the light absorption coefficient. Disregarding the small differences in the effective sound velocities from sample to sample, Eq. (11) shows that for a fixed laser energy $\Delta\omega$ depends only on the absorption coefficient. Using Eq. (11) we calculate a contribution to the linewidth due to absorption that decreases from 0.7 cm^{-1} to 0.5 cm^{-1} as the superlattice period decreases from 232 Å to 63 Å. The small decrease is due to the larger thickness of the silicon layers relative to the germanium layers in the small period samples. It contradicts the experimental evidence that the linewidth increases with decreasing period. The contribution to the linewidth due to absorption is shown by the hatched regions in Fig. 8. While the absorption can explain the width of the low-frequency peaks, the high-frequency Raman peaks are much broader than the prediction of Eq. (9). Most important, the absorption contribution to the linewidth does not scale with ω and can therefore not explain the differences in the width of the ω_{-1} and ω_{+1} peaks in the same sample.

A second possible mechanism to account for the broadening of the Raman peaks is variations in the superlattice period due to inhomogeneities of the total film thickness within the area illuminated by the laser beam. Away from the edges of the mini-Brillouin-zone we have from Eq. (5) the following relationship between the frequency shift $\delta\omega$ caused by a change δd in the period

$$\left[1+m\frac{qd}{2\pi}\right]\frac{\delta\omega}{\omega}=\frac{\delta d}{d}\ , \tag{12}$$

where m is again the branch index. Assuming that the relative variations of the film thickness are the same for all samples, $\delta\omega/\omega$ is constant as long as $qd/2\pi \ll 1$. For $\lambda=6471$ Å this condition is fulfilled for $d \lesssim 100$ Å. This would result in a linear relationship ($\nu=1$) between linewidth and ω.

To test this possibility we recorded Raman spectra from different points on the surface of a particular sample (Fig. 9). In our Raman measurements the laser beam is concentrated on a (1.2 ± 0.2)-mm-long linear trace by a cylindrical lens. One spectrum was recorded on the

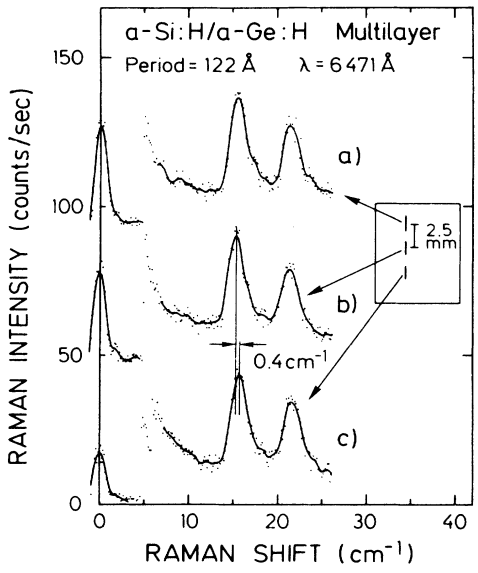

FIG. 9. Raman spectra from folded phonons measured at different points on the sample surface as shown in the inset. The small changes in the phonon frequency is attributed to variations in the superlattice period along the surface.

center of the sample [Fig. 9(b)] and two others at points approximately 2.5 mm away from the center [Figs. 9(a) and 9(c)]. The frequency of the folded-phonon excitations varied slightly with the position: it was smallest at the center of the sample [Fig. 9(b)] and ~ 0.4 cm^{-1} higher away from the center [Figs. 9(a) and 9(c)]. Over the width of the laser spot (1.2 mm) the corresponding contribution to the relative Raman linewidth $d\omega/\omega$ amounts to no more than 0.01, a factor of 5 too small to explain the broadening observed in Fig. 8. From these data we conclude that variations in the film thickness over distances of a few mm are not responsible for the observed line broadening. Measurements with a stylus-type profilometer confirmed that the thickness variations along the surface on a length scale between 50 μm and 1 mm are at least a factor of 4 smaller than those necessary to explain the linewidth.

We now consider the broadening effects that are related with the propagating characteristics of the acoustic phonons on a microscopic scale. In a perfect periodic and harmonic structure the phonons created in the Stokes light scattering process have an infinite lifetime and therefore well-defined energies. Deviations from this condition lead to lifetime reductions with a concomitant spread in the phonon energy. We shall discuss the line broadening in terms of the phase coherence length of the phonons l which characterizes the spatial extension over which the phase coherence of an acoustic mode is maintained.[5] If the phonon wave vector is smaller than $1/l$, the displacement field can be expressed by

$$u(q,z) \cong e^{iqz} e^{-z/l} , \tag{13}$$

where z is the propagation direction perpendicular to the layers. We neglect in this expression the mixing of modes from neighboring branches that is important only at the boundaries of the superlattice mini-Brillouin-zone. The light scattered by the phonon is related to the square of the Fourier transform of Eq. (13) and the intrinsic width Γ (in wave numbers) of the Raman peaks is then given by:[29]

$$\Gamma = \frac{v_{\text{eff}}}{\pi l c} . \tag{14}$$

The ratio of the linewidth to the mean frequency (in cm^{-1}) $\bar{\omega} = v_{\text{eff}}/cd$ is then

$$\frac{\Gamma}{\bar{\omega}} = \frac{d}{\pi l} . \tag{15}$$

In order to have the folding of the LA dispersion relation in the superlattice it is necessary that $l \gg d$, so that several phonon reflections at the superlattice interfaces can coherently interfere. In fact, one obtains from Eq. (15) $d/l \simeq 0.2$ for the frequency range shown in Fig. 8. Furthermore, for the 6471-Å laser light, with which our measurements were made, $1/q \simeq 250$ Å $< l$ for all samples with a period larger than 50 Å. This assures the validity of Eq. (13) for superlattice periods within this range. Using Eqs. (10) and (14) and assuming an effective sound velocity of 6.6×10^5 cm/s for all superlattices, the frequency dependence of l is found to be

$$l = [(2.4 \pm 0.4) \times 10^{-4} \text{ cm}] \left[\frac{\omega}{1 \text{ cm}^{-1}} \right]^{-\nu} \tag{16}$$

with $\nu = 1.3 \pm 0.1$.

To obtain additional information about the scattering processes responsible for the reduction of the phonon lifetime, we measured the temperature dependence of the Raman lines. Due to the decreasing intensity of the signal with temperature, these measurements were restricted to temperatures above that of liquid nitrogen. Figure 10 shows the Raman spectra of sample no. 138 ($d = 63$ Å) and of sample no. 136 ($d = 122$ Å) measured at 120 and 300 K. The solid lines in this figure are Lorentzian fits to the data points that yield the linewidths shown next to each peak. These linewidths were not corrected for the spectrometer resolution of 1.8 ± 0.1 cm^{-1}, as determined from the FWHM of the laser line. For the small period sample [no. 138 in Figs. 10(a) and 10(b)] no significant change in linewidth with temperature was observed. The frequencies of the folded phonons in this sample lie in the frequency range where the linewidth begins to increase rapidly with frequency (see Fig. 6). The temperature-independent linewidth indicates that the phonons are elastically scattered in this frequency range. For the sample with $d = 122$ Å per period of Figs. 10(c) and 10(d), the linewidth decreases with decreasing temperature. The folded phonon frequencies of this sample lie in the middle frequency range of Fig. 8. We followed the temperature dependence of the linewidth in this sample in Fig. 11, where the Raman spectra were measured with a spectrometer resolution of 2.1 ± 0.1 cm^{-1}. The linewidth is approximately constant for temperatures above 300 K and, as the temperature decreases, it approaches the spectrometer resolution. This behavior is displayed by both peaks of the folded-phonon doublet. It should be men-

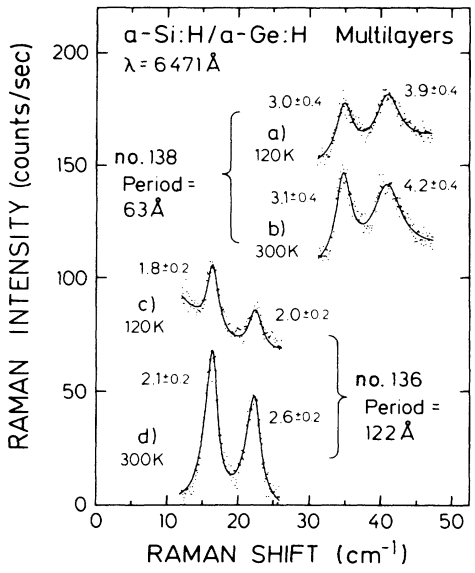

FIG. 10. Raman spectra from folded phonons in superlattices with periods of 63 and 122 Å recorded at different temperatures. The solid lines are Lorentzian fits to the data points; the linewidth (in cm^{-1}) is shown next to each peak.

tioned that the contribution of the absorption to the linewidth is so small that the decrease of the absorption coefficient with temperature cannot account for the linewidth reduction.

The correlation between linewidth and phonon frequency may thus be divided into three different regions. For low frequencies the linewidth is determined by the broadening of the light wave vector due to absorption (see Fig. 8). As the frequency increases an intermediate frequency range is reached where $l \sim \omega^{-\nu}$ or $l \sim d^{\nu}$ with $\nu = 1.3 \pm 0.1$, as indicated by Eq. (16). Because the number of interfaces that a phonon traverses per unit time is also proportional to d, it is tempting to associate the

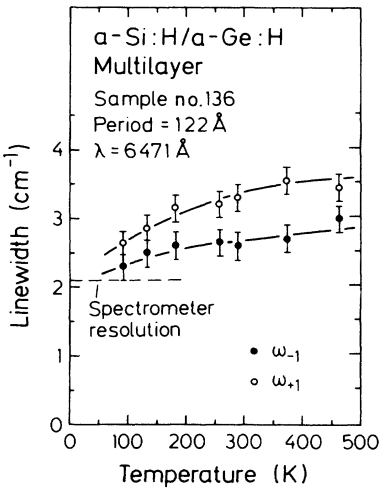

FIG. 11. Width of folded-LA-phonon Raman lines as a function of temperature. The linewidth was not corrected for the spectrometer resolution of 2.1 cm^{-1}.

reduction in the phonon coherence length to scattering processes occurring at the interfaces. However, purely elastic scattering by defects at the interfaces cannot account for the temperature dependence of the phonon coherence length, which arises from the interaction of the folded acoustic phonon with other excitations.

For even higher frequencies ($\geqq 40$ cm^{-1}), the linewidth increases rapidly with frequency. This range corresponds to the low frequency tail of the TA-like Raman peak from a-Ge:H, as shown in Fig. 6(a). The phase coherence length of the TA-like vibrations in germanium seems to be smaller than that of the LA folded phonons. Indeed, as shown in Fig. 6(a), the folded LA phonon excitations are still observable, indicating a certain degree of phase coherence, while the TA-like vibrations appear as a broad background. This is a consequence of the loss of phase coherence and the resulting relaxation of the wave vector conservation rule for Raman scattering. We ascribe the linewidth of the folded phonons in this energy range to a mixing of modes with LA and TA character.

VI. CONCLUSIONS

We have investigated the vibrational spectra of a-Si:H/a-Ge:H superlattices by Raman spectroscopy. In the range of high-frequency optical vibrations the Raman spectrum is the incoherent sum of the scattering intensities of the individual bonds probed by the laser light. It contains therefore contributions from homopolar Si—Si and Ge—Ge bonds within the layers, and from heteropolar Si—Ge bonds at the interfaces. By comparing the Raman spectra of the superlattices with those of unstructured silicon, germanium, and a silicon-germanium alloy we calculated the "spectroscopic" thicknesses of each layer. The thicknesses determined in this way agree with those obtained from the analysis of the growth rates of the films. This procedure is a particularly useful one for the study of interfaces and interface mixing. The calculated number of heteropolar bonds per interface and per unit area (3.5×10^5 cm^{-2}) is equal to the number of similar bonds present in a (7.5±2)-Å-wide a-$Si_x Ge_{1-x}$ layer with $x = 0.57$.

The low frequency part of the Raman spectrum of the superlattices shows well-defined structures corresponding to the excitation of zone-folded LA phonons. From the analysis of their frequencies as a function of superlattice period and laser energy we determine the LA dispersion relation. We conclude that the corresponding dispersion relation for a-Si:H and a-Ge:H are linear for wave vectors up to at least 10% of the Brillouin-zone of the corresponding crystals. As the phonon frequency increases, the dispersion relation acquires an imaginary component due to the increasing localization of the acoustic phonons. The phonon coherence length determined from the linewidth of the folded phonon peaks varies as $\omega^{-\nu}$ with $\nu = 1.3 \pm 0.1$ in the frequency range from 10 and 40 cm^{-1}. For higher frequencies, the coherence length decreases rapidly to the point that folded-phonon excitations are hardly observed above ~ 40 cm^{-1}. This corresponds to a transition from the region of low frequency extended acoustic phonons to high frequency localized vibrations.

Finally, these results demonstrate that amorphous superlattices are a convenient system for probing interfaces and high frequency acoustic vibrations in amorphous materials by means of light scattering. This technique allows the study of the phonon propagation in amorphous materials in a frequency and temperature range that is not normally directly accessible by other methods such as ultrasound propagation,[30] thermal conductivity,[31] or phonon transmission experiments.[32]

ACKNOWLEDGMENTS

The authors would like to thank K. Winer and K. Syassen for helpful discussions and comments on the preparation of the manuscript. We also acknowledge the technical support of W. Neu and F. Kübler in the sample preparation and of M. Siemers, P. Wurster, and H. Hirt in the Raman measurements.

[1]B. Abeles and T. Tiedje, Phys. Rev. Lett. **51**, 2003 (1983).
[2]N. Ibaraki and H. Fritzsche, Phys. Rev. B **30**, 5791 (1984).
[3]M. Hirose and S. Miyasaki, J. Non-Cryst. Solids **66**, 327 (1984).
[4]P. Santos, M. Hundhausen, and L. Ley, Phys. Rev. B **33**, 1516 (1986).
[5]M. Brodsky, in *Light Scattering in Solids,* edited by M. Cardona (Springer-Verlag, Berlin, 1975), p. 205.
[6]P. D. Persans, A. F. Ruppert, B. Abeles, and T. Tiedje, Phys. Rev. B **32**, 5558 (1985).
[7]D. D. Allred, J. Gonzalez-Hernandez, O. V. Nguyen, D. Martin, and D. Pawlik, J. Mater. Res. **1**, 468 (1986).
[8]M. Grimsditch, W. Senn, G. Winterling, and M. Brodsky, Solid State Commun. **26**, 229 (1978).
[9]J. Sapriel, J. C. Michel, J. C. Toledano, R. Vacher, J. Kervarec, and A. Regreny, Phys. Rev. B **28**, 2007 (1983).
[10]C. Colvard, R. Merlin, M. V. Klein, and A. C. Gossard, Phys. Rev. Lett. **45**, 298 (1980).
[11]P. Santos, M. Hundhausen, and L. Ley, J. Non-Cryst. Solids **77&78**, 1069 (1985).
[12]M. Hundhausen, Ph.D. thesis, University of Stuttgart, 1986.
[13]K. D. Mackinzic, J. Hanna, J. R. Eggert, Y. M. Li, Z. L. Sun, and W. Paul, J. Non-Cryst. Solid **77&78**, 881 (1985); M. Stutzmann (private communication).
[14]J. C. Knights, R. A. Lugan, M. P. Rosenblum, R. A. Street, D. K. Biegelsen, and J. A. Reimer, Appl. Phys. Lett. **38**, 331 (1981).
[15]R. A. Street, J. C. Knights, and D. K. Biegelsen, Phys. Rev. B **18**, 1880 (1978).
[16]F. J. Kampas, J. Appl. Phys. **54**, 2276 (1983).
[17]R. Alben, J. E. Smith, M. H. Brodsky, and D. Weaire, Phys. Rev. Lett. **30**, 1141 (1973). See also J. Tauc, in *Amorphous and Liquid Semiconductors,* edited by J. Tauc (Plenum, London, 1974), p. 159.
[18]G. Lucovsky and W. B. Pollard, in *The Physics of Hydrogenated Amorphous Silicon II,* edited by J. D. Joannopoulos and G. Lucovsky (Springer-Verlag, Berlin, 1984), p. 301.
[19]F. Yndurain, Phys. Rev. Lett. **37**, 1062 (1976).
[20]S. M. Prokes and F. Spaepen, Appl. Phys. Lett. **47**, 234 (1986).
[21]M. Hundhausen, P. Santos, L. Ley, F. Habraken, W. Beyer, R. Primig, and G. Gorges, J. Appl. Phys. **61**, 556 (1987).
[22]C. Colvard, T. A. Grant, M. V. Klein, R. Merlin, R. Fisher, H. Morkoc, and A. C. Gossard, Phys. Rev. B **31**, 2080 (1985).
[23]J. Sapriel, B. Djafari-Rouhani, and L. Dobrzynski, Surf. Sci. **126**, 197 (1983).
[24]B. A. Auld, *Acoustic Fields and Waves in Solids,* (Wiley-Interscience, New York, 1973), Vol I.
[25]R. E. Camley, B. Djafari-Rouhani, L. Dobrzynski, and A. A. Maradudin, Phys. Rev. B **27**, 7318 (1983).
[26]S. M. Rytov, Sov. Phys. Acoust. **2**, 68 (1956).
[27]M. Born and K. Huang, *Dynamical Theory of Crystal Lattice* (Clarendon, Oxford, 1954).
[28]J. R. Sandercock, Phys. Rev. Lett. **28**, 237 (1972); in *Light Scattering in Solids III,* edited by M. Cardona and G. Güntherodt (Springer-Verlag, Berlin, 1982), p. 173.
[29]W. F. Love, Phys. Rev. Lett. **31**, 822 (1973).
[30]See, for instance, B. Golding, J. E. Graebner, B. I. Halperin, and R. J. Schutz, Phys. Rev. Lett. **30**, 223 (1973).
[31]M. P. Zaitlin and A. C. Anderson, Phys. Rev. B **12**, 4475 (1975).
[32]W. Dietsche and H. Kinder, in *Phonon Scattering in Condensed Matter,* edited by H. J. Maris (Plenum, New York, 1979), p. 37; or M. Rothenfusser, W. Dietsche, and H. Kinder, Phys. Rev. B **27**, 5196 (1983).